

# Ultra-Wideband RCS Reduction of Metasurface Antenna Based on Spoof Surface Plasmon Polariton and Transmission

Si-Jia LI<sup>1</sup>, Xiang-Yu CAO<sup>1</sup>, He-Xiu XU<sup>2</sup>, Zhao ZHANG<sup>1</sup>,  
Yu-Long ZHOU, Jiang-Feng HAN<sup>1</sup>, Chen ZHANG

<sup>1</sup> Information and Navigation College, Air Force Engineering University, No.1 FengHao Road, Xi'an 710077, China

<sup>2</sup> Missile Institute, Air Force Engineering University, Xi'an 710051, China

lsj051@126.com, gjgj9694@163.com, hxxuellen@gmail.com, bjzhangzhao323@126.com,  
511043618@qq.com, hanjimkl@163.com, xue320long@sina.cn

Submitted November 30, 2017 / Accepted March 6, 2018

**Abstract.** *In this paper, a metasurface antenna with ultra-broadband radar cross section (RCS) reduction was systematically presented and evaluated based on the spoof surface plasmon polariton (SSPP) and transmission. A circular metasurface consisted of twelve gradually increasing two-sided metallic grooves and an ultra-thin dielectric substrate. The evolutions of the dispersion characteristic and near electric-field distributions were adequately demonstrated based on SSPP in simulation. Furthermore, the SSPP metasurface had been loaded on a common waveguide slot antenna. The simulation and laboratory measurements were performed to characterize RCS reduction, radiation patterns and scattering performance. A prototype of metasurface antenna has been fabricated and measured to demonstrate the characteristics. Experimental data were carried out to verify the simulation results and the measured results showed that the metasurface antenna exhibited ultra-wideband RCS reduction from 1 GHz to 10 GHz.*

## Keywords

Ultra-broadband, radar cross section reduction, metasurface antenna, spoof surface plasmon polariton

## 1. Introduction

Over the last decade, the radar cross section (RCS) reduction of antenna has been a topic of immense strategic interest for the researchers. For out-of-band frequencies, it is well known that the RCS of antenna/array can be significantly reduced by placing the periodic resistive surface [1], [2] and suitably shaped band-pass radome, such as frequency selective surfaces [3], [4]. To reduce RCS of antenna, the radome is usually designed and fabricated as the frequency selective filter which allows the working

frequencies to pass with the least amount of insertion loss and reflects out of band incidences. Generally, the in-band RCS is dominated by the antenna itself and it can't be reduced by the radome [1]. Consequently, it is an important research aspect to reduce in-band RCS of antenna.

Fortunately, the application of metamaterial or metasurface as the available methods has been introduced to achieve the in-band RCS reduction of antenna [5–7]. Several metamaterial absorbers, which have been designed, fabricated and used as the reflected or radiated ground for a composition of antenna, have been paid attention to in-band RCS reduction [8–11]. The electromagnetic band-gap (EBG) is applied for in-band RCS reduction because the surface currents of antenna are absorbed. In aspect of waveguide slot antenna, EBG as a radar absorbing material loaded with lumped resistances is investigated to reduce in-band RCS in [12], where the EBG overcomes the thickness restrict of Salisbury screen and the lumped resistive elements were used to better match the impedance of free space, and as chief contributor of absorption. The in-band RCS of microstrip antenna is significantly reduced by EBG in [13]. Then, perfect metamaterial absorbers with different structures have been designed and applied for in-band RCS reduction of antenna or array in [14]. Moreover, as the application of the principle of passive cancellation for electromagnetic wave, the artificial magnetic conductor (AMC) and perfect electric conductor (PEC) surfaces were combined together for in-band RCS reduction and radiation improvement of waveguide slot antenna and microstrip antenna [15]. Then, two AMCs with different metamaterial structures were theoretically analyzed and easily implemented using common printed circuit board fabrication methods for ultra-thin and broadband metamaterial design [16]. Similarly, a metamaterial surface with orthogonal arrangement was proposed to broadband RCS reduction for a waveguide slot antenna based on AMC with complementary split ring resonator structure in [16]. Nevertheless, it is obvious that the RCS is reduced in boresight direction but

increased in other directions. Recently, it is a novel method that the polarization conversion metasurface with multi-band and broadband has been introduced to reduce RCS of microstrip antenna [17–19]. These methods have been used to reduce the RCS of the antenna or array antennas.

Nowadays, the spoof surface plasmon polaritons (SSPPs) have attracted intensive attention due to their attractive and remarkable capability of guiding electromagnetic wave into sub-wavelength scales and localizing electromagnetic fields on metal surface [20]. Different SSPP devices have been proposed in microwave frequency [21–23]. On this basis, the aim of this work is to provide a new waveguide slot metasurface antenna loaded with SSPP metasurface to obtain an ultra-wide band RCS reduction. The SSPP metasurface is composed of twelve gradually increasing two-sided metallic grooves and an ultra-thin dielectric substrate. The characteristics of waveguide slot metasurface antenna have been thoroughly illustrated by simulation. Comparing to the common antenna, the presented results of the metasurface antenna exhibit an ultra-wide band RCS reduction and the wider beam width due to the SSPP waves and the transmission for the incidence. As a partial experimental validation, the attractive metasurface antenna easily implemented using the common printed circuit board fabrication method has been fabricated and measured by employing the free-space test method in a microwave anechoic chamber. Experiments are in good agreement with results obtained from simulations.

## 2. Design and Analysis of Metasurface Based on SSPP

The detailed optimum dimensions of the presented circular metasurface are shown in Fig. 1. The cell is composed of the gradually increasing two-sided leaf-shaped metallic grooves array and an ultra-thin flexible dielectric substrate in Fig. 1(a). The two-sided leaf-shaped metallic grooves are only etched on the bottom of the substrate. The metal is copper with the conductivity of  $5.8 \times 10^7$  S/m and the thickness is 0.036 mm. RT/Duroid 5880 ( $\epsilon_r = 2.2$  and  $\tan\delta = 0.001$ ) is used as the substrate with the thickness of 0.5 mm. As shown in Fig. 1(b), the length of a unit cell for the two-sided leaf-shaped metallic grooves array is defined as follows

$$\begin{bmatrix} X_i \\ Y_i \\ Z \end{bmatrix} = a_i \cos(2t) \begin{bmatrix} \sin t \\ \cos t \\ 0 \end{bmatrix}, \quad t \in [0.25\pi, 0.75\pi], \quad (1)$$

$$a_i = 11 - 0.8i, [\text{mm}] \quad i = 0, \dots, 11 \quad (2)$$

where  $a_i$  is a coefficient. The length  $r_1$  and the width  $w$  of the substrate are 60 mm and 28 mm, respectively. The other optimized results are given in Fig. 1. The metasurface is simulated and optimized using the commercial finite element method (FEM) solver by ANSOFT HFSS 15.0.

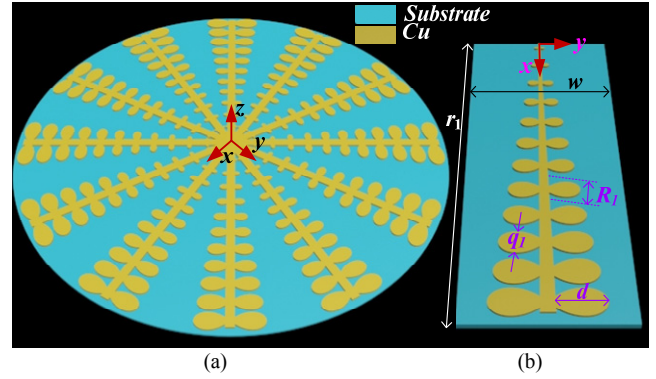
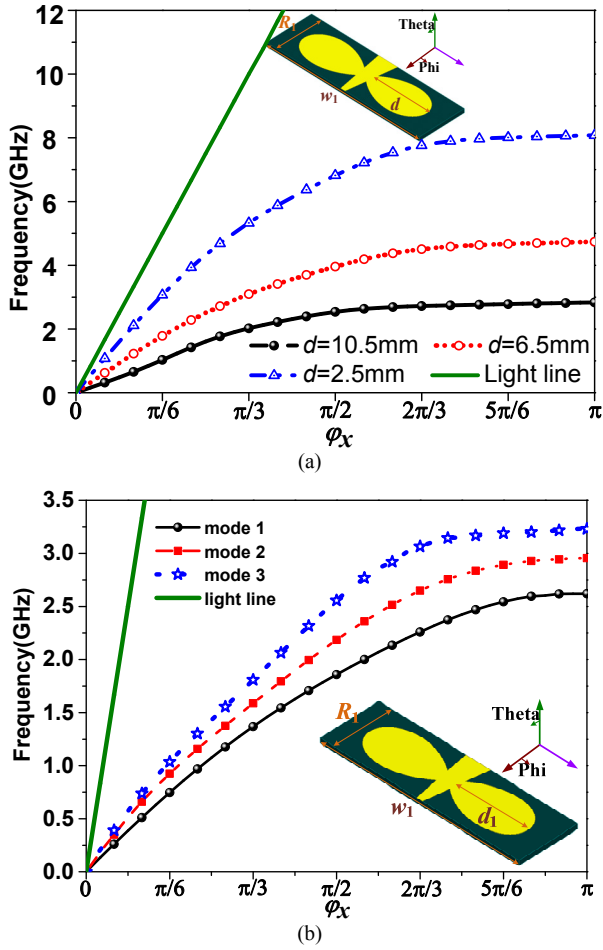


Fig. 1. (a) Geometry of the proposed circular metasurface based on the SSPP and (b) the unit cell of circular metasurface based on the spoof surface plasmon polaritons.  $r_1 = 60$  mm,  $w = 28$  mm,  $a_0 = 11$  mm,  $R_1 = 5$  mm.

For the metasurface, the excitation mechanism of SSPP means a kind of conversion from the spatial propagating waves to the SSPP waves. Considering the TM polarized waves impinging at the two-sided leaf-shaped grooves array with parallel momentum  $k_x$ , the reflectance can be calculated based on the boundary conditions. Since the surface modes are considered, we have  $k_x > k_0$ . On conditions of  $\lambda \gg (Q - q_1)$  and  $\lambda \gg Q$  ( $\lambda$  is the working wavelength), the desired dispersion relation of the leaf-shaped metallic grooves array can be achieved from the locations of divergences in  $x$  direction. With the first-order approximation,  $k_x$  can be expressed as [11], [23]

$$k_x = k_0 \sqrt{1 + \frac{(Q - q_1)^2}{Q^2} \tan^2(k_0 d)}. \quad (3)$$

For the condition of  $0 < k_0 d < \pi/2$ ,  $k_x$  is a real number and  $k_x > k_0$ , and hence the velocity of SSPPs is lower than light. From (3), it can be found that  $k_x$  is proportional to  $d$  within propagation band and the asymptotic frequency is mainly controlled by the depth  $d$  for surface waves. In other words,  $k_x$  will be enlarged by increasing the depth of leaf-shaped metallic grooves. Accordingly, the SSPPs propagate more slowly but confine more tightly to the gradually increasing two-sided leaf-shaped metallic grooves array. The Eigen-mode simulation is conducted by Eigen-mode solver for illustrating the analysis of (3). In simulation, the boundary conditions as “open” have been set to simulate the real space, and we set the boundaries at large distances from the metal structure for avoiding spurious reflections. In order to study the effect on the dispersion property, dispersion curves of the first Eigen mode with different depths  $d$  have been simulated in Fig. 2(a). We can see that the dispersion curves shift to higher frequency as depth  $d$  decreases from 10.5 mm to 2.5 mm. The cut-off frequencies are respectively 2.65, 4.72 and 7.97 GHz with the depths  $d$  of 10.5, 6.5 and 2.5 mm. The cut-off dispersion curve is much close to the light line as the width  $d$  decreases to zero. In design of the SSPP metasurface, the depth  $d$  of 10.5 mm has been chosen to design the novel waveguide slot metasurface antenna with low RCS. The dispersion curves of the first three Eigen modes with



**Fig. 2.** Simulated dispersion curves. (a) The simulated dispersion curves of the first Eigen modes for SSPPs with different depths. (b) Simulated dispersion curves of different modes with depth  $d = 10.5$  mm.  $w_1 = 28$  mm,  $a_0 = 11$  mm,  $R_1 = 5$  mm.

$d = 10.5$  mm are shown in Fig. 2(b). It is observed that the dispersion curves shift to higher frequency as the modes increase and the cut-off frequencies are 2.65, 2.92 and 3.22 GHz for mode 1, 2 and 3, respectively. In our design, the basic mode is TE<sub>10</sub> mode for the presented waveguide. Consequently, the depth  $d$  of 10.5 mm with the cut-off frequency of 2.65 GHz of mode 1 was applied in the metasurface.

The far-field scattering performances of the proposed metasurface have been investigated to illustrate the conversion of scattering direction from the incident wave to the spoof surface plasmon polariton wave. As shown in Fig. 3, the monostatic radar cross section (MRCS) and bistatic radar cross section (BRCS) at 2 GHz are given with the x-polarized incident wave. It can be seen that the remarkable MRCS reduction can be obtained from 1 GHz to 10 GHz especially, with the peak value of 26.9 dB of MRCS reduction at 2.0 GHz. It is noted that the RCS reduction from 1 GHz to 2.65 GHz is mainly attributed to SSPP and that in the other frequency band is caused by transmission for the EM wave leak from slots in proposed metasurface. From Fig. 3(b), (c), we can see that the beam direction of BRCS for metasurface is along x-axes but that for perfect electric

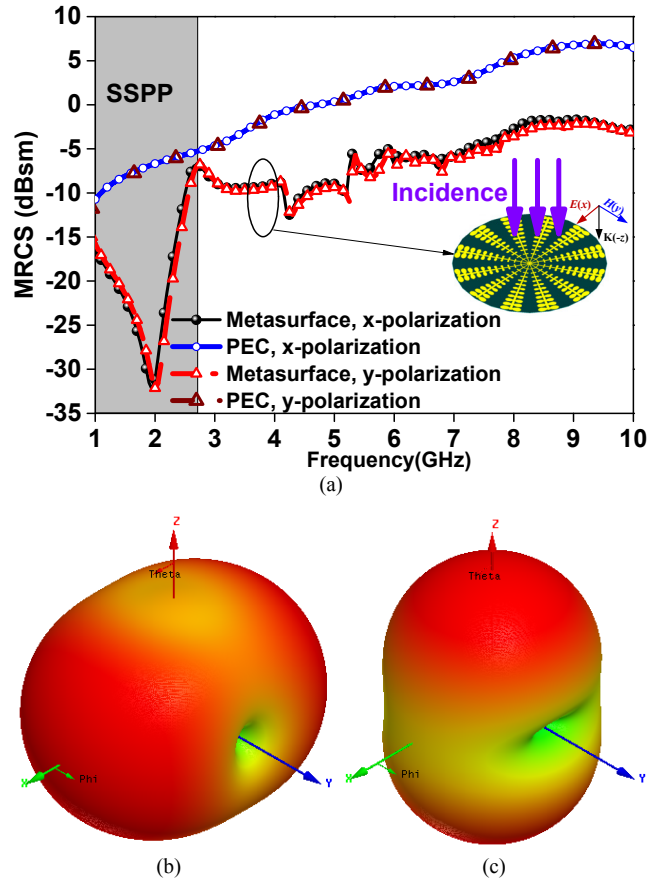


**Fig. 3.** The MRCS from 1 GHz to 10 GHz and BRCS at 2 GHz of the metasurface and the PEC when the y-polarized incident wave propagates along  $-z$  direction. (a) MRCS results. (b) BRCS of the metasurface. (c) BRCS of the PEC with the same condition.

conductor (PEC) is along z-axes because the metasurface converts the x-polarized incident wave to SSPP wave at 2.0 GHz.

### 3. Design, Simulation and Analysis of Metasurface Antenna

Figure 4 shows the proposed metasurface antenna and the common guidewave slot antenna (common antenna). The common antenna in Fig. 4(b) is usually composed of a thin copper aperture etched radiating slot of  $26 \times 2$  mm<sup>2</sup> and a C-band standard waveguide for feeding the antenna. The height of the copper for the common antenna is 0.5 mm. In the present investigation, the circular metasurface which consists of twelve gradually increasing two-sided leaf-shaped metallic grooves array mounted on a circular thin substrate of RT/duroid5880 with the same slot in center and the C-band standard waveguide for feeding is designed to enhance the surface waves as shown in Fig. 1(a). The metal is copper with the conductivity of  $5.8 \times 10^7$  S/m and its thickness is 0.036 mm. The substrate is RT/duroid5880 with the thickness of 0.5 mm. It is necessary to note that a copper of 30 mm  $\times$  6 mm is only accreted on the bottom of the substrate.

To illustrate the performance of the antenna, Figure 5 shows the comparison of  $S_{11}$  and radiation patterns at 5.5 GHz for the common antenna and the proposed metasurface antenna. Table 1 gives the details about the parameters of the radiation performances for metasurface and common antennas. We can see that the impedance bandwidth is 10.3% with  $S_{11} < -10$  dB from 5.16 GHz to 5.72 GHz for the metasurface antenna and that is 9.3% for common antenna from 5.34 GHz to 5.86 GHz as shown in Fig. 5(a). The impedance bandwidth is enhanced due to the coupling effects between the slot and the metasurface. From Fig. 5(b), we observe that the cross polarization (x-polar) of E-plane with the main lobe remains less than  $-35$  dB for metasurface and common antenna. As shown in

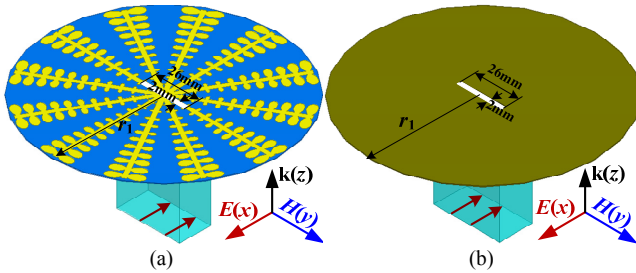


Fig. 4. Geometry of (a) metasurface antenna and (b) common antenna with the parameter.  $r_1 = 60$  mm.

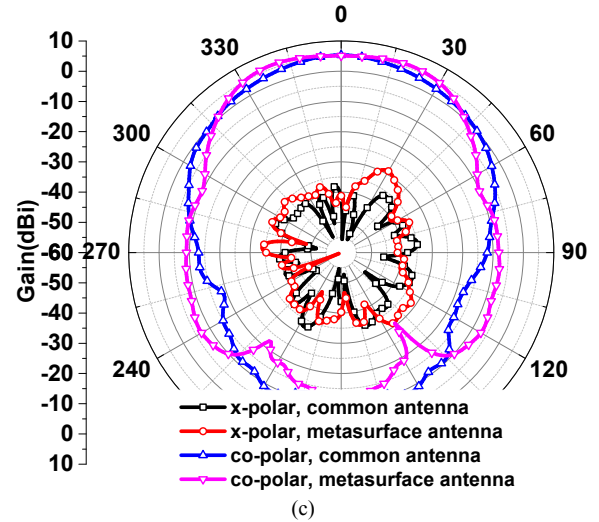
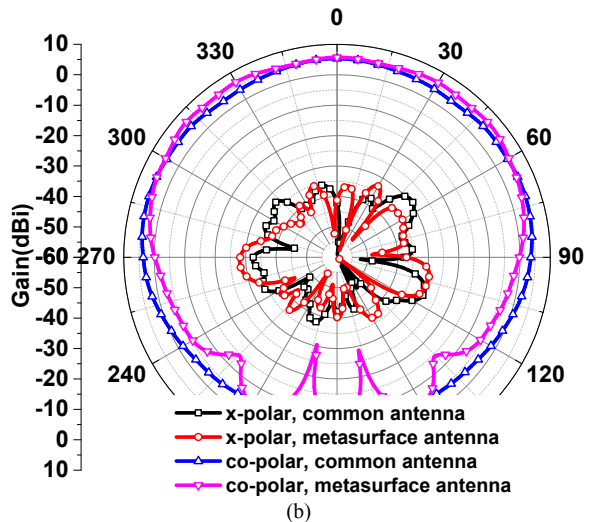
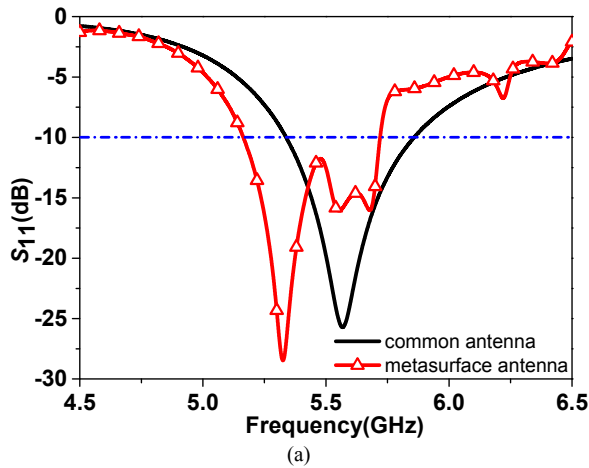


Fig. 5. Simulated  $S_{11}$  and radiation patterns of E-plane and H-plane at frequency of 5.5 GHz for the metasurface antenna and common antenna. (a) Simulated results of  $S_{11}$ . (b) Radiation patterns of E-plane. (c) Radiation patterns of H-plane.

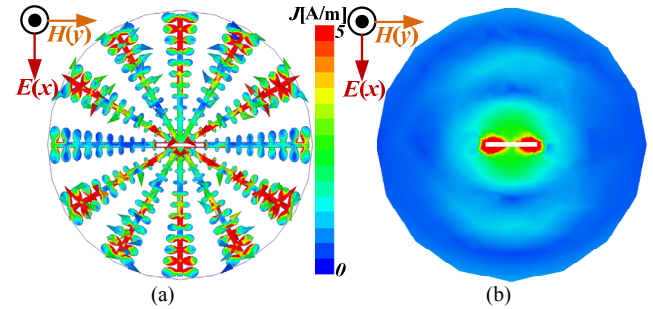


Fig. 6. Surface current distributions of metallic structure for the (a) metasurface antenna and (b) common antenna at 5.5 GHz.

Tab. 1, the beam width of E-plane is increased from 155 deg for the common antenna to 182 deg for the metasurface antenna and that of H-plane is shifted from 60 deg for the common antenna to 71 deg for the metasurface antenna. These phenomena are mainly attributed to the gain reduction which is caused by the transmission of the radiated electromagnetic wave from the slots of the metasurface antenna. From Fig. 2, we can see that the cut-off frequencies are respectively 4.72 and 7.97 GHz with the depths  $d$  of 6.5 and 2.5 mm and the cut-off frequency would decrease as the mode increased. Meanwhile, the impedance bandwidth of the metasurface antenna is from 5.16 GHz to 5.72 GHz. So the secondary reason of the gain reduction is the SSPP waves excited by the circular metasurface. As shown in Fig. 6, it can be seen that stronger surface current density is exhibited for the metasurface antenna and less surface current density is performed for copper ground plane. In conclusion, the proposed metasurface not only enhanced the impedance bandwidth but also widened the beamwidth of E-plane and H-plane for the antenna.

Figure 7 gives the simulated results of MRCS and BRCS for the metasurface antenna and the common antenna



	Impedance Bandwidth		Gain(dBi)	Radiated Beam Width	
	$S_{11} < -10$ dB(GHz)	bandwidth		E-plane(Deg)	H-plane(Deg)
Metasurface antenna	5.16~5.72	10.3%	4.8	182	71
Common antenna	5.34~5.86	9.3%	5.6	155	60

Tab. 1. The comparison of the radiation characteristics for metasurface and common antenna.

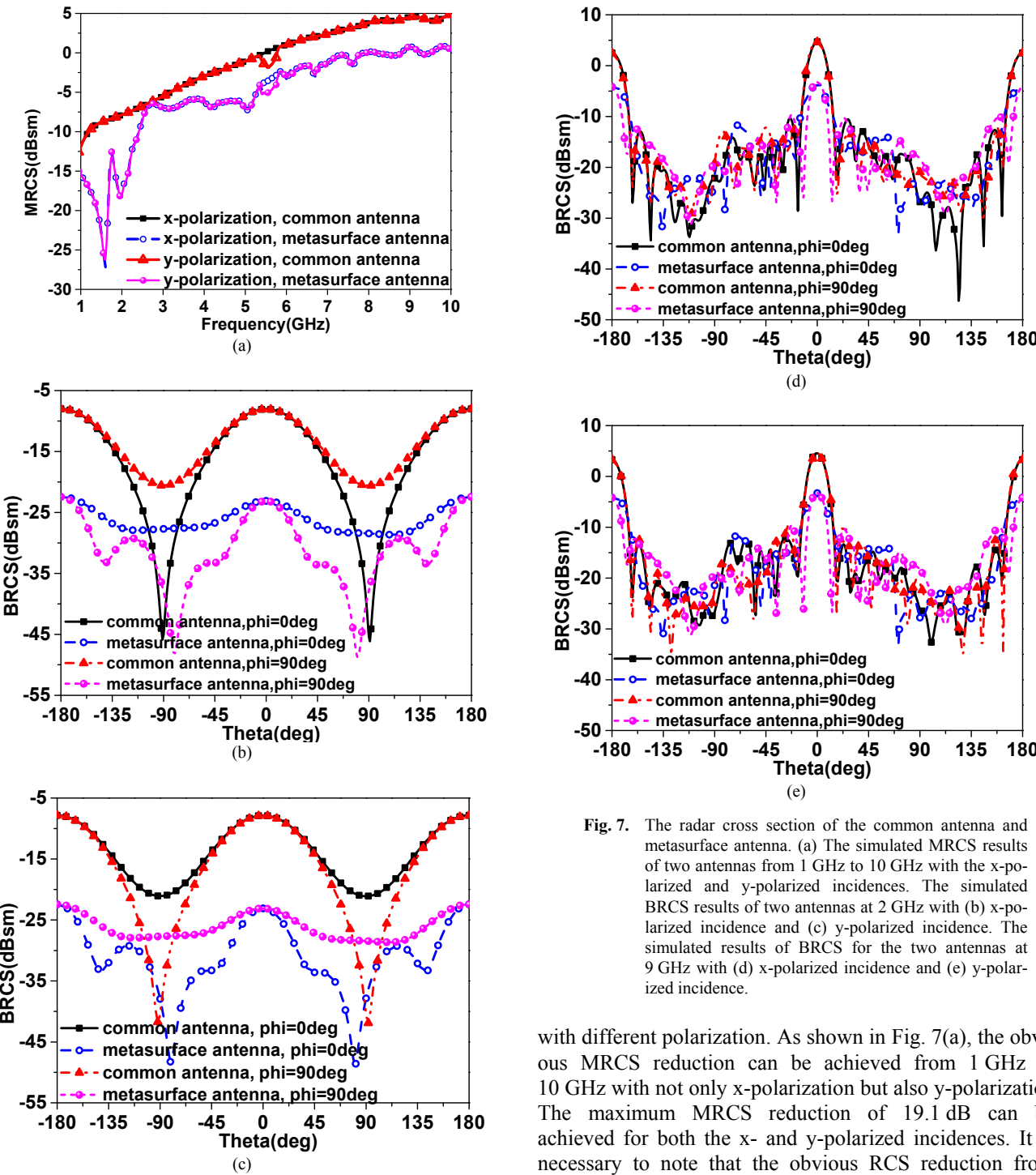


Fig. 7. The radar cross section of the common antenna and metasurface antenna. (a) The simulated MRCS results of two antennas from 1 GHz to 10 GHz with the x-polarized and y-polarized incidences. The simulated BRCS results of two antennas at 2 GHz with (b) x-polarized incidence and (c) y-polarized incidence. The simulated results of BRCS for the two antennas at 9 GHz with (d) x-polarized incidence and (e) y-polarized incidence.

with different polarization. As shown in Fig. 7(a), the obvious MRCS reduction can be achieved from 1 GHz to 10 GHz with not only x-polarization but also y-polarization. The maximum MRCS reduction of 19.1 dB can be achieved for both the x- and y-polarized incidences. It is necessary to note that the obvious RCS reduction from

1 GHz to 2.65 GHz is mainly caused by the translation from incident waves to SSPP waves. And while, the broadband RCS reduction in the other frequency is caused by transmission for the EM wave leak from slots of the metasurface antenna. The more RCS reduction peaks at low frequency for the metasurface antenna which are different from that for the proposed metasurface are attributed to the coupling effects between the radiating slot and the twelve gradually increasing two-sided leaf-shaped metallic grooves array. We can see that there are several differences of RCS results with the different polarized incident waves for antennas which are due to the polarization of the antenna.

#### 4. Fabrication and Measurement of Metasurface Antenna

To validate the performances mentioned above, a metasurface antenna device and a common antenna device with the same dimensions have been fabricated using the common printed circuit board processing technology. The dielectric substrate was chosen as RT/duroid5880 boards with the thicknesses of 0.5 mm. The metal DMSRs and ground were made of 0.036 mm-thick copper layers. The devices have been tested by employing the free-space test method in a microwave anechoic chamber. A vector network analyzer of Agilent N5230C and two standard-gain horn antennas were used to transmit and receive the electromagnetic waves for RCS simulation. Two antenna devices with same area were placed vertically in the center of a turntable to ensure that the incidences were similar to a plane wave for measuring scattering characteristics.

The measured results of the  $S_{11}$  and radiation patterns are shown in Fig. 8. More in details, the metasurface antenna device achieved the broad bandwidth from 5.21 GHz to 5.78 GHz with  $S_{11} < -10$  dB compared to the common antenna device which exhibited the impedance bandwidth from 5.35 GHz to 5.78 GHz in the same standard in Fig. 8(a). As shown in Figs. 8(b) and 8(c), it is observed that the cross polarizations (x-polar) of the E-plane and the H-plane with the main lobe remain less than  $-38$  dB for these metasurface and common antennas. The beamwidth of E-plane is increased from 147 deg for the common antenna to 176 deg for the metasurface antenna and that of H-plane is shifted from 62 deg for common antenna to 73 deg for metasurface antenna. The measured results agree well with the simulated results.

The experimental results of RCS reduction are shown in Fig. 9. More in details, the metasurface device exhibited an ultra-broadband low scattering from 1 GHz to 10 GHz of obvious RCS reduction for different polarized waves. Moreover, several RCS reduction peaks could be obtained from Fig. 9. The similar RCS reduction cures for different polarized incidences indicated the insensitive polarization for the metasurface antenna device. The experimental results agree well with the simulated results. The RCS reduc-

tion peaks for x-polarized and y-polarized incidences were 19.2 dB and 16.9 dB at 1.22 GHz and 2.24 GHz, respectively. It is noted that the differences between the simulation and the measurement are addressed by the gaps between the metasurface and the C-band standard waveguide, and the tolerance of the fabrication and the measurement.

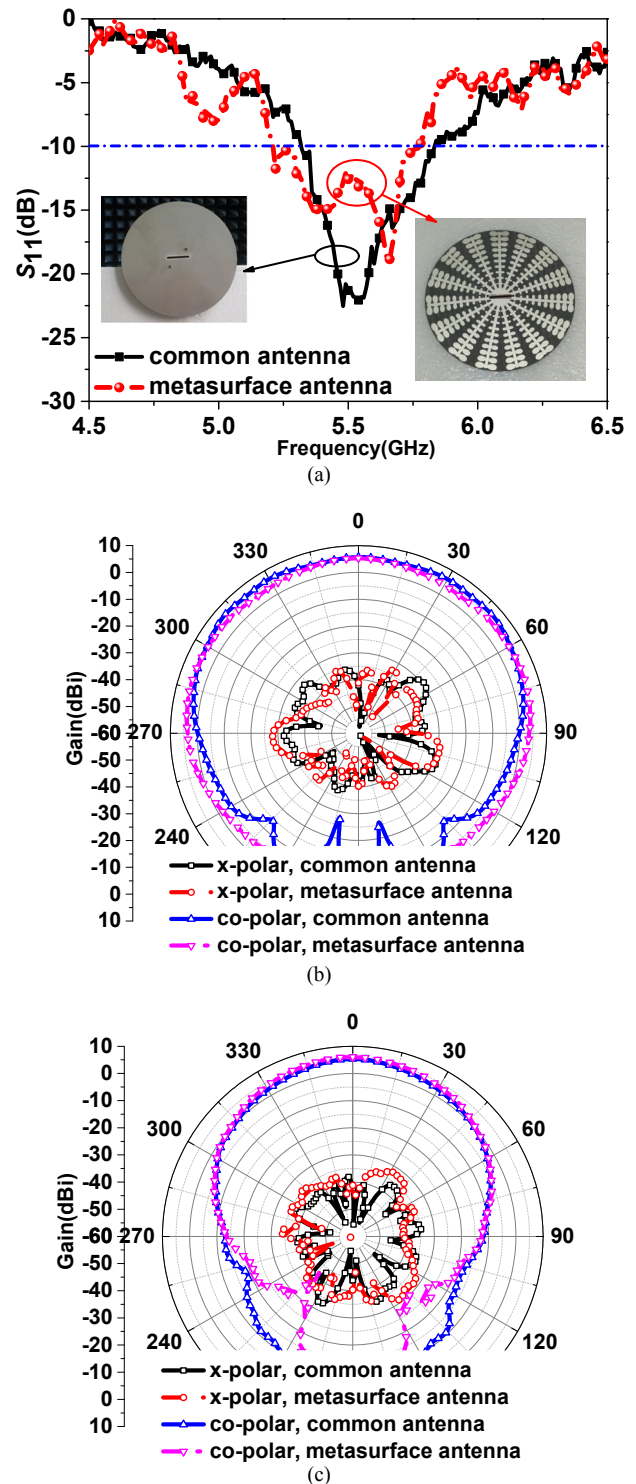


Fig. 8. Measured results of (a)  $S_{11}$  and radiation patterns of (b) E-plane and (c) H-plane at frequency of 5.5 GHz for the metasurface antenna device and the common antenna device.

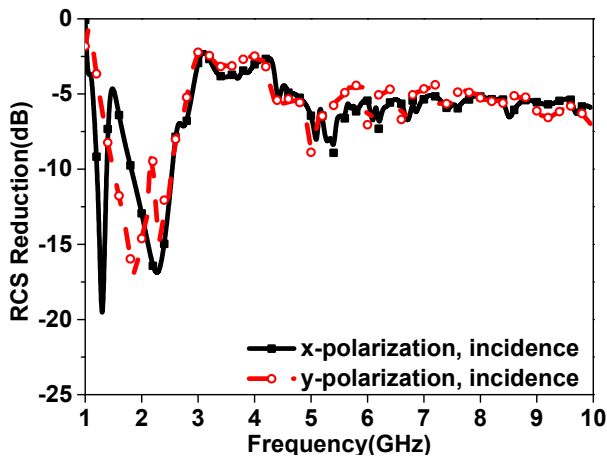


Fig. 9. Experimental results of RCS reduction for the metamaterial screen device with different polarized incidences.

## 5. Conclusion

In conclusion, we proposed a metasurface antenna based on the spoof surface plasmon polariton (SSPP) and transmission. The proposed antenna composed of the metasurface and the C-band standard waveguide for feeding the antenna. The beamwidth has been broadened and the radar cross section was reduced due to the SSPP and the transmission. The surface current distributions and scattering parameters were introduced to demonstrate the SSPP and transmission. The simulated and experimental results indicated that the RCS reduction peaks 19.2 dB and 16.9 dB can be obtained respectively at 1.22 GHz and 2.24 GHz for different polarization. The experiments were carried out to verify the simulation results and measured results showed that the metasurface antenna exhibited ultra-wideband RCS reduction from 1 GHz to 10 GHz.

## Acknowledgments

This work was supported in part by the National Natural Science Foundation of China under Grant Nos. 61271100, 61471389, 61501494, 61671464 and 61701523, in part by the Natural Science Foundational Research Fund of Shaanxi Province under Grant No. 2017JM6025, in part by the Young Talent Fund of University Association for Science and Technology in Shaanxi, China (No. 20170107), in part by the Innovative Talents Cultivate Program of Shaanxi Province under grant No. 2017KJX-24. The authors also thank the reviewers for their valuable comments.

## References

[1] GENOVESI, S., COSTA, F., MONORCHIO, A. Wideband radar cross section reduction of slot antennas arrays. *IEEE Transactions*

*on Antennas and Propagation*, 2014, vol. 62, no. 1, p. 163–173. DOI: 10.1109/TAP.2013.2287888

- [2] MONTI, A., SORIC, J., BARBUTO, M., et al. Mantle cloaking for co-site radio-frequency antennas. *Applied Physics Letters*, 2016, vol. 108, no. 11, p. 113502-5. DOI:10.1063/1.4944042
- [3] ZHOU, H., QU, S.-B., LIN, B.-Q., et al. Filter-antenna consisting of conical FSS radome and monopole antenna. *IEEE Transactions on Antennas and Propagation*, 2012, vol. 60, no. 6, p. 3040–3045. DOI: 10.1109/TAP.2012.2194648
- [4] TURPIN, J. P., SIEBER, P. E., WERNER, D. H. Absorbing ground planes for reducing planar antenna radar cross-section based on frequency selective surfaces. *IEEE Antennas and Wireless Propagation Letters*, 2013, vol. 12, no. 1, p. 1456–1459. DOI: 10.1109/LAWP.2013.2288682
- [5] PENDRAY, J. B., SCHURIG, D., SMITH, D. R. Controlling electromagnetic fields. *Science*, 2006, vol. 312, no. 5781, p. 1780 to 1782. DOI: 10.1126/science.1125907
- [6] LI, S., GAO, J., CAO, X., et al. Wideband, thin, and polarization insensitive perfect absorber based the double octagonal rings metamaterials and lumped resistances. *Journal of Applied Physics*, 2014, vol. 116, p. 043710. DOI: 10.1063/1.4891716
- [7] JIA, Y., LIU, Y., GUO, J., et al. Broadband polarization rotation reflective surfaces and their applications to RCS reduction. *IEEE Transaction on Antennas and Propagation*, 2016, vol. 64, no. 1, p. 179–185. DOI: 10.1109/TAP.2015.2502981
- [8] PAN, W., HUANG, C., PU, M., et al. Combining the absorptive and radiative loss in metasurface for multi-spectral shaping of the electromagnetic scattering. *Scientific Reports*, 2016, vol. 6, p. 21462. DOI: 10.1038/srep21462
- [9] EDALATI, A., SARABANDI, K. Wideband, wide angle, polarization independent RCS reduction using nonabsorptive miniaturized-element frequency selective surfaces. *IEEE Transactions on Antennas and Propagation*, 2014, vol. 62, no. 2, p. 747–753. DOI: 10.1109/TAP.2013.2291236
- [10] LI, S., GAO, J., CAO, X., et al. Loading metamaterial perfect absorber method for radar cross section reduction based on the surface current distribution of guidewave slot array antennas. *IET Microwaves, Antennas and Propagation*, 2015, vol. 9, no. 5, p. 399–406. DOI: 10.1049/iet-map.2014.0490
- [11] LI, S., GAO, J., CAO, X., et al. Multiband and broadband polarization-insensitive perfect absorber devices based on a tunable and thin double split-ring metamaterial. *Optics Express*, 2015, vol. 23, no. 3, p. 3523–3533. DOI: 10.1364/OE.23.003523
- [12] LI, Y.-Q., ZHANG, H., FU, Y.-Q., YUAN, N.-C. RCS reduction of ridged waveguide slot antenna array using EBG radar absorbing material. *IEEE Antennas and Wireless Propagation Letters*, 2008, vol. 7, no. 1, p. 473–476. DOI: 10.1109/LAWP.2008.2001548
- [13] LI, S., GAO, J., CAO, X., et al. Broadband and high-isolation dual-polarized microstrip antenna with low radar cross section. *IEEE Antennas and Wireless Propagation Letters*, 2014, vol. 13, p. 1413–1416. DOI: 10.1109/LAWP.2014.2339933
- [14] ZHANG, C., CAO, X., GAO, J., et al. Low RCS and broadband ME dipole antenna loading artificial magnetic conductor structures. *Radio Engineering*, 2017, vol. 26, no. 1, p. 38–44. DOI: 10.13164/re.2017.0038
- [15] TAN, Y., YAN, N., YANG, Y., et al. Improved RCS and efficient waveguide slot antenna. *Electronics Letters*, 2011, vol. 47, no. 10, p. 582–583. DOI: 10.1049/el.2011.0842
- [16] IRIARTE GALARREGUI, J. C., TELLECHEA PEREDA, A., MARTINEZ DE FALCON, J. L., et al. Broadband radar cross-section reduction using AMC technology. *IEEE Transactions on Antennas and Propagation*, 2013, vol. 61, no. 12, p. 6136–6143. DOI: 10.1109/TAP.2013.2282915

- [17] LIU, Y., LI, K., JIA, Y., et al. Wideband RCS reduction of a slot array antenna using polarization conversion metasurfaces. *IEEE Transactions on Antennas and Propagation*, 2016, vol. 64, no. 1, p. 326–331. DOI: 10.1109/TAP.2015.2497352
- [18] YIN, J. Y., WAN, X., ZHANG, Q., et al. Ultra-wideband polarization-selective conversions of electromagnetic waves by metasurface under large-range incident angles. *Scientific Reports*, 2015, vol. 5, p. 12476. DOI: 10.1038/srep12476
- [19] GAO, X., HAN, X., CAO, W. P., et al. Ultra-wideband and high-efficiency linear polarization converter based on double v-shaped metasurface. *IEEE Transaction on Antennas and Propagation*, 2015, vol. 63, no. 8, p. 3522–3530. DOI:10.1109/TAP.2015.3434 392
- [20] MA, H. F., SHEN, X., CHENG, Q., et al. Broadband and high-efficiency conversion from guided waves to spoof surface plasmon polaritons. *Laser and Photonics Reviews*, 2014, vol. 8, no. 1, p. 146–151. DOI: 10.1002/lpor.201300118
- [21] VASA, P., WANG, W., POMRAENKE, R., et al. Optical stark effects in-aggregate-metal hybrid nanostructures exhibiting a strong exciton-surface-plasmon-polariton interaction. *Physical Review Letters*, 2015, vol. 114, no. 3, p. 036802. DOI: 10.1103/PhysRevLett.114.036802
- [22] WAN, X., LI, Y. B., CAI, B. G., et al. Simultaneous controls of surface waves and propagating waves by metasurfaces. *Applied Physics Letters*, 2014, vol. 105, no. 12, p. 121603. DOI: 10.1063/1.4896540
- [23] LI, S.-J., GAO, J., CAO, X.-Y., et al. Hybrid metamaterial device with wideband absorption and multiband transmission based on spoof surface plasmon polaritons and perfect absorber. *Applied Physics Letters*, 2015, vol. 106, no. 18, p. 181103. DOI: 10.1063/1.4919789

## About the Authors ...

**Si-Jia LI** was born in Xi'an, Shaanxi province, P.R. China in 1987. He received the B. Eng. degree in Electronics and Information Engineering from Guangxi University, Nanning, China, in 2009 and the M. Eng. degree in Information and Telecommunication Engineering from Air Force Engineering University, Xi'an China, in 2011. He received the Ph.D. degree in Electronic Science and Technology at the Information and Navigation College, Air Force Engineering University in 2015. From December 2015 to December 2017, he was a senior researcher and a lecturer in the Air Force Engineering University. Now he is an associate professor in the Air Force Engineering University. He has been working with the Military Communication and Navigation

Antenna and EMC Lab., since 2012. His research activity has been focused in the metamaterial, the broadband and fractal perfect metamaterial absorber and its application for RCS reduction of antennas. He has authored and coauthored more than 60 scientific papers in major journals and international conferences. He received the excellent Master's dissertation in 2012. He is awarded the 2012, 2013 and 2014 Best Student Paper Prize (First Prize) of the National Graduate Mathematical Modeling Contest in Shanghai in December 2012, in Changsha in December 2013 and in Tianjin in December 2014. He was a recipient of the Best Paper Award at the Forth National Doctor Forum Symposium on Information Science of China in Guangzhou in October 2013. He is awarded the excellent student in the 2014 national summer school of the Microwave Material and Components. He is a reviewer of the Applied Physics Letter, Journal of Applied Physics, IEEE Transactions on Microwave Theory & Techniques, IEEE Transactions on Antennas & Propagation, IEEE Antennas Wireless Propagation Letter, Electronic Letters and Microelectronics Journal.

**Xiangyu CAO** received the B. Sc and M.A. Sc degrees from the Air Force Missile Institute in 1986 and 1989, respectively. She joined the Air Force Missile Institute in 1989 as an assistant teacher. She became an associate professor in 1996. She received Ph.D. degree in the Missile Institute, Air Force Engineering University in 1999. From 1999 to 2002, she was engaged in postdoctoral research in Xidian University, China. She was a Senior Research Associate in the Dept. of Electronic Engineering, City University of Hong Kong from June 2002 to Dec 2003. She is currently a professor of Information and Navigation College, Air Force Engineering University of CPLA. She is the IEEE senior member from 2008. She has authored and coauthored more than 200 technical journal articles and conference papers, and holds one China soft patent. She is the coauthor of two books entitled Electromagnetic Field and Electromagnetic Wave, and Microwave Technology and Antenna published in 2007 and 2008, respectively. Her research interests include smart antennas, electromagnetic metamaterial and their antenna applications, and electromagnetic compatibility. She is a reviewer of the Applied Physics Letter, Journal of Applied Physics, IEEE Transactions on Antennas & Propagation, and IEEE Antennas Wireless Propagation Letter.